Characteristics and mechanism of lake water changes in the Tianshan region during 2002–2022

Zhiqiang Wen, Shuang Yi and Wenke Sun*

College of Earth and Planetary Sciences, University of Chinese Academy of Sciences, Beijing 100049, China.

Correspondence: *sunw@ucas.ac.cn

Abstract: The variations in the lake water storage in the Tianshan region are an important indicator of climate change and play a key role in understanding the hydrological mass balance. Based on altimetry and satellite gravity, we investigated the spatiotemporal characteristics of the lake water storage changes during 2002–2022, and examined the contributions and proportions of all of the hydrological components to the mass balance. The results indicate that the total water storage of the lake complex showed an increasing rate (0.73±0.10 Gt/a). We found two abrupt wet periods in 2010 and 2016 (the regional total mass increased by 65.73 Gt and 67.35 Gt, respectively), which were reflected not only by the lake water storage but also by the soil moisture, snow water, and even GNSS displacement fields. Compared with their contributions to the mass (22% and 14%), the variations in lake area were remarkably slight (0.01% and 0.014%). Among the hydrological components, the soil moisture played a dominant role, and the contribution of the snow accumulation changes was also considerable. The mass anomalies were closely related to the precipitation caused by the increase of water vapor content, which was further associated with the occurrence of ENSO events ($r=0.55$, $p<0.01$). The results revealed that the long-term trend of the GNSS vertical displacements exhibited a better stability after the load correction was applied, which could reflect the long-term ground deformation more accurately.

This study contributes to our understanding of the complex hydrological and tectonic processes in the Tianshan region.

Plain Language Summary: Tianshan lake water storage variations are vital for climate change assessment and hydrological balance. Using altimetry and satellite gravity during 2002–2022, we studied Tianshan Lake storage changes. Total lake water storage showed an increasing trend of 0.73±0.10 Gt/a. Two wet periods occurred in 2010 and 2016, impacting not only lake storage but also soil moisture, snow water, and GNSS displacement fields. Regional mass increased by 65.73 Gt and 67.35 Gt. Lake area changes were minor (0.01% and 0.014%) but contributed significantly (22% and 14%) to mass. Soil moisture dominated among hydrological components, and snow accumulation changes were noticeable. Mass anomalies correlated closely with precipitation, linked to El Niño–Southern Oscillation events ($r=0.55$, $p<0.01$). Intensified El Niño led to increased Tianshan water vapor and precipitation. We calculated elastic vertical displacements from mass changes and corrected GNSS data. Long-term vertical displacements showed better stability after correction. This study enhances our knowledge of complex hydrological and tectonic processes in Tianshan.

Key Points

(1) The lake water storage increased, and two anomalous periods occurred, as verified in other hydrological components

(2) The ENSO-related precipitation anomaly was the main cause of the two anomalous mass periods in the Tianshan region

(3) Load deformation correction is of great importance for maintaining the long-term stability of the GNSS displacement field

1 Introduction

As an essential reservoir of surface water on Earth, lakes are highly sensitive to climate change, and their water storage variations are considered to be indicators of climate change (Adrian et al., 2009; Zhang et al., 2019; Woolway et al., 2020). There are a large number of lakes distributed globally, and approximately 53% of the large lakes, especially those located within continents, experienced a continuous decrease in water storage from 1992 to 2020 (Yao et al., 2023). Research findings clearly demonstrate that the fluctuations in lake water storage primarily stem from natural factors, including precipitation (Zhang et al., 2017; Wang et al., 2022a) and evaporation (Zhao et al., 2022), as well as human activities (Grant et al., 2021). Therefore, monitoring the dynamic changes in lake water storage is crucial for understanding the global water cycle and its driving factors (Xu et al., 2022b). Additionally, lakes are a significant component of regional water storage, and accurate monitoring and estimation of their mass changes contribute to a better understanding of the regional mass balance.

The Tianshan region is situated in the arid and semi-arid zone within the interior of the Eurasian continent and has a typical temperate continental climate. It is influenced by three monsoon belts, namely the southwest, Indian, and northwestern monsoons, but is primarily influenced by the northwestern monsoon. The main sources of the water storage in the lake complex in the Tianshan region are generally believed to be precipitation and glacial meltwater. The study area encompasses the entire Tianshan mountain range and its surrounding regions. In

this study, we focused on the region enclosed by the black dashed line in Figure 1. Although this region includes numerous lakes of different sizes, for the sake of convenience, we selected eight representative large lakes, namely Balkhash, Kapchagay, Issykkul, Sasykkol, Alakol, Saysan, Ulungur, and Bosten (labeled with numbers in Figure 1), which occupied an area of ~35,000 km^2. These lakes contribute significantly to the total water storage of the lake complex. The study area consists of the Tianshan snow-covered area and the lake complex, which encompasses the hydrological variations within the region. This study area selection facilitated the comprehensive analysis of the high mountain snowmelt, lake water level changes, and their relationships with meteorological factors.

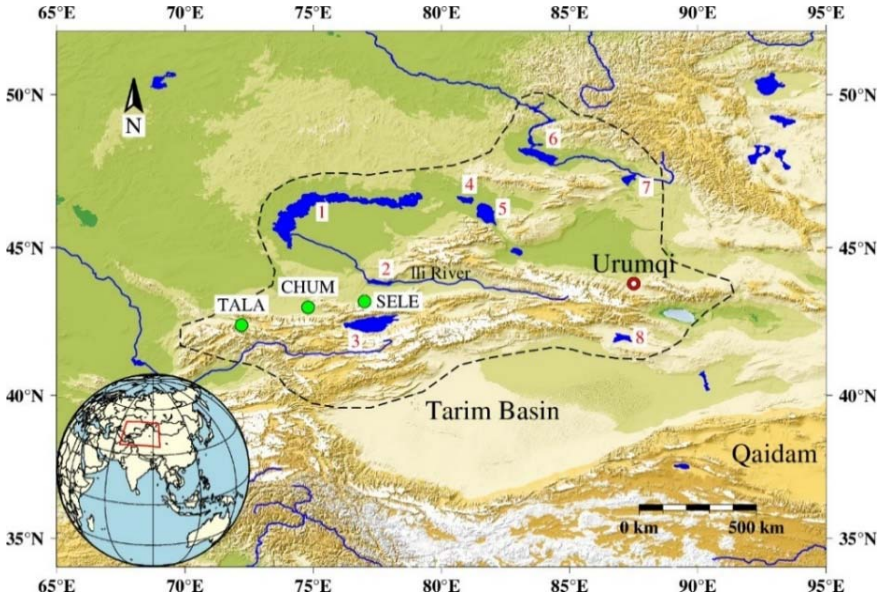

Figure 1. Study area (black dashed line) and geographic overview of the lake complex in the Tianshan region. 1 - Balkhash, 2 - Kapchagay, 3 - Issykkul, 4 - Sasykkol, 5 - Alakol, 6 - Zaysan, 7 - Ulungur, 8 - Bosten. The green dots denote the locations of GPS stations.

The Tianshan region in China contains a considerable number of lakes, forming a relatively

concentrated lake complex. This area serves as a typical region for studying lake level and/or water storage variations. Research has revealed that extreme precipitation events in the Tianshan region are closely related to the Indian Ocean summer monsoon (Zhong et al., 2017) and abnormal westerly winds (Yi et al., 2016). Zhang et al. (2023) pointed out that the main sources of water of the lakes located at middle and low elevations in the Tianshan region are precipitation and glacial meltwater, while the lakes at high elevations are primarily replenished by glacial meltwater. Therefore, the lake water storage changes in the Tianshan region are directly associated with ice and snow melting caused by climate variations in the region. Additionally, lakes located in densely populated areas are more susceptible to the influence of human activities (Li et al., 2003). Currently, research on the lakes in the Tianshan region has mainly focused on long-term monitoring of lake water levels and surface areas. Yi et al. (2016) studied the water level changes in the lake complex in the Tianshan region and identified a mass anomaly period in 2010. They attribute this anomaly to the dominant influence of the northwestern monsoon. Liu et al. (2019) utilized moderate resolution imaging spectroradiometer (MODIS) 500 m resolution global water body data to study the interannual and seasonal variations in the surface areas of 14 lakes in Central Asia from 2001 to 2016, as well as the influencing factors. Their results revealed that the lakes located in plain areas experienced a reduction in surface area, while the high mountain lakes exhibited expansion. Zhang et al. (2022a) used multisource satellite data to investigate the water level changes in Lake Issyk-Kul from 1958 to 2020. Their results indicate that before 1998, human activities were the main cause of the continuous decline in the water level. However, after 2000, the increases in rainfall and glacial meltwater, as well as the decrease in water usage, led to short-term recovery of the lake's water level. The above studies indicate that there is significant

interannual variability in the water volume of the lakes in the Tianshan region. Investigating this can help us understand and explain the characteristics of climate change and human activities in the Tianshan region.

The main observational parameters reflecting lake water storage changes are the lake water level and lake surface area, both of which can be obtained through remote sensing techniques and in situ water level measurements. In situ water level monitoring is the traditional method for monitoring the water levels of reservoirs and lakes, but it can be affected by complex terrain conditions and incomplete data recording. In addition, in situ water level measurements cannot cover inland lakes located in remote and inaccessible regions, resulting in a lack of long-term and effective water level change data. With the emergence of remote sensing measurement techniques, represented by altimetry satellites, many researchers have opted to use these methods instead of traditional water level monitoring approaches due to their regular data acquisition periods and wide data coverage range (Jiang et al., 2017). Remote sensing measurements, which offer advantages such as all-weather capability, comprehensive coverage, and high efficiency, have been widely employed in lake hydrological research. Currently, there are two main types of measurement methods: geometric measurements and physical measurements. Geometric measurements refer to the use of optical imagery combined with spatial geodetic measurement techniques to obtain changes in the lake surface area. For instance, researchers use optical remote sensing data such as Landsat data to monitor global surface water area changes (Yao et al., 2019) or regional surface water area changes (Olthof et al., 2015; Zhang et al., 2017; Xu et al., 2021). They then utilize altimetry techniques to monitor changes in the lake levels (Zhang et al., 2011; Zhang et al., 2019; Xu et al., 2022), thereby obtaining the variations in the lake water storage.

Physical measurement methods refer to direct detection the mass changes of lake water storage using gravity detection satellites, such as the Gravity Recovery and Climate Experiment (GRACE) (Xu et al., 2020), as well as the gravity changes generated by variations in reservoirs (Yi et al., 2017; Tangdamrongsub et al., 2019). The results obtained from both geometric and physical measurements can mutually corroborate each other.

In addition to a lake complex, the Tianshan region contains continuously melting glaciers and snow, which are significant contributors to the lake water storage variations (Yi et al., 2016). The lake variations in the Tianshan region are closely linked to the water contributions from glacier and snow melt (Wang et al., 2013; Rinzin et al., 2023). Therefore, studying the changes in glaciers and snow enables us to gain a deeper understanding of the mechanisms behind lake variations. Regarding glacier monitoring, because glaciers are located in high-altitude areas, there are limited results from in situ observations, which can lead to deviations. Therefore, global and regional glacier monitoring mainly relies on the following types of satellite remote sensing observation methods: high-resolution digital elevation model (DEM) differencing (Gardelle et al., 2012; Gardelle et al., 2013), estimating glacier thickness changes using altimetry satellites (Kääb et al., 2012; Kääb et al., 2015; Wang et al., 2017a), and directly obtaining mass changes using gravity satellites such as GRACE (Matsuo and Heki, 2010; Jacob et al., 2012; Yi and Sun, 2014). Additionally, changes in the snowline have been used to infer glacier variations (Barandun et al., 2021). Due to observational limitations, many researchers have primarily focused on studying the long-term trends of glaciers. For instance, Hugonnet et al. (2021) provided the longest time span for global glacier melting rates, and reported annual global glacier melting of 267 ± 16 Gt. At the regional scale, Wang et al. (2017b) and Wang and Sun (2022b) reported continuous annual glacier

148 elevation changes in the Asian high mountain regions, while Barandun et al. (2021) reported
149 annual glacier mass balance results for the Tianshan region from 1999 to 2017. With the
150 development of satellite technology, obtaining glacier mass changes with a higher time resolution
151 will become possible.

152 Furthermore, the lakes in the Tianshan region exhibit significant mass fluctuations, and
153 together with other hydrological components such as soil moisture and groundwater, they impose
154 a substantial load effect on surface deformation observations in this region. This phenomenon is
155 included in global navigation satellite system (GNSS) observations (Heki, 2004; Heki and Arief,
156 2021; White et al., 2022). This interferes with our ability to extract the signals of long-term
157 tectonic motions. To study tectonic movements effectively, it is essential to accurately account for
158 the effects of these surface loads (Rao and Sun, 2022). Pan et al. (2019) utilized global positioning
159 system (GPS) and GRACE data to obtain the three-dimensional deformation field in the Tianshan
160 region. Pan et al. (2021) presented the most comprehensive distribution of the vertical
161 displacement field in mainland China, corrected the vertical displacement due to surface loads
162 using GRACE data, and subsequently obtained information about tectonic movements. Wu et al.
163 (2022) also combined levelling measurements and GNSS data to obtain high-precision vertical
164 displacement data for the Tibetan Plateau region. Wen et al. (2023) constructed a global mass
165 change model and used Green's function integration method to calculate the vertical displacement
166 due to surface loads in mainland China. They found that the GNSS vertical velocity field in the
167 Tianshan region is primarily driven by extensive glacier melt-induced surface mass changes,
168 which result in rapid uplift of Earth's surface.

169 The above-mentioned research indicates that currently, researchers have mainly utilized

multisource space geodetic techniques to study the glacier mass balance in the Tianshan region (Farinotti et al., 2015; Brun et al., 2017; Barandun et al., 2021) or have conducted studies from the perspective of tectonic movements to investigate the three-dimensional deformation and orogenic motion in the Tianshan region (Li et al., 2022; Pan et al., 2023). However, the spatiotemporal distribution characteristics of the lake water storage changes in the Tianshan region are not yet well understood. Questions related to the hydrological components contributing to water storage changes in the lake complex, their relationship with changes in the precipitation in the region, the total mass balance of the region, and the main physical mechanisms driving water storage changes in the lake complex are all significant scientific questions that warrant attention.

Therefore, the goal of this study was to utilize multisource remote sensing observation data, including altimetry and GRACE data, to investigate the spatiotemporal distribution of the water storage changes in the lake complex in the Tianshan region from 2002 to 2022. Additionally, GNSS displacement observations were employed to investigate the characteristics of the surface load deformation. The goals were to quantify and analyze the lake water changes during two anomalous periods, to quantitatively calculate the contributions of the lake water, soil moisture, snow water, glacial mass changes, and other hydrological components to the total surface mass change monitored by GRACE and finally to explore and analyze the physical mechanisms underlying the two occurrences of abnormal mass changes.

2 Datasets and methods

2.1 Datasets

2.1.1 Global surface water area dataset

To build a global mass redistribution model and calculate the load deformation, as well as to extract the relevant lake water area, in this study, we used a global surface water area dataset that includes statistical data on the location, extent, and temporal distribution of the surface water from 1984 to 2020 (Jean-Francois et al., 2016). This dataset was generated using 4,453,989 images acquired by Landsat-5, 7, and 8 satellites from March 16, 1984, to December 31, 2021, and each pixel was classified as water or non-water using an expert system. The data products are divided into two categories: monthly variations during the entire period and temporal changes during two separate periods (1984–1999 and 2000–2020). The dataset contains 442 images, one for each month from March 1984 to December 2021. In this study, we obtained the lake area changes from 2002 to 2020 using the Google Earth Engine (GEE) and fitted the water level–area relationship of altimetry data to estimate the water volume changes of the lake complex from 2002 to 2022.

2.1.2 Altimetry data

Most of the lakes in the study area are covered by altimetry data, and the water level data products were obtained from several websites (https://ipad.fas.usda.gov/cropexplorer/global_reservoir/, https://dahiti.dgfi.tum.de/en/map/, http://hydrolare.net/catalogue.php). Multiple sources of altimetry satellite data were used, including data from European remote sensing satellite (ERS)-1, Geosat follow-on (GFO), ERS-2, JASON-1, ENVISAT, and others. For all of the lakes, remote sensing was utilized to obtain the lake area changes, and the water level data obtained through altimetry were combined to construct the lake-water level area curve. After data screening and outlier removal of the products from different organizations and systematic error adjustment, we obtained water level monitoring data for all of the lakes in the study area. The basic information about the lake complex is presented in

213 Table 1.

214 Table 1 Summary of the basic information about the lake complex in the Tianshan region

No.	Lake	longitude (°E)	latitude (°N)	Level Method	Water type
1	Balkhash	75.81	46.64	Altimetry	Lake
2	Kapchagay	77.63	43.80	Altimetry	Lake/reservoir
3	Issykku	77.3	42.4	Altimetry	Lake
4	Sasykkol	80.97	46.59	Altimetry	Lake
5	Alakol	81.75	46.14	Altimetry	Lake
6	Zaysan	83.88	48.02	Altimetry	Lake/reservoir
7	Ulungur	87.32	47.28	Altimetry	Lake
8	Bosten	87.05	42	Altimetry	Lake

215 2.1.3 GNSS data

216 To analyze the ground deformation characteristics in the Tianshan region, in this study, we
217 utilized GNSS data from the Nevada Geodetic Laboratory
218 (http://geodesy.unr.edu/NGLStationPages/GlobalStationList), which are in the IGS2008 reference
219 frame. Due to various factors such as receiver malfunctions and changes in the surface
220 environment during GPS operations, long-term GPS stations may experience data gaps. To
221 address this issue, the TSAnalyzer software was employed to remove anomalies and outliers from
222 the GNSS time-series data (Wu et al., 2018).

223 2.1.4 Precipitation data

224 Precipitation data were one of the key datasets used in this study. We adopted the Global
225 Precipitation Climatology Centre (GPCC) model. The GPCC was established in 1989 in response
226 to the World Meteorological Organization's (WMO) request and is operated by the German
227 Meteorological Service (Deutscher Wetterdienst). The center's mission is to analyze and establish

a global rainfall database based on observed rainfall data for daily and monthly precipitation at the Earth's surface. It is the world's largest precipitation database. All GPCC products are based on observed global land surface gridded precipitation datasets, which use a large number of station observations to compute the grid values. Several reanalysis datasets have been compared, and it has been reported that the GPCC precipitation model is better suited for long-term precipitation change studies in Central Asia (Hu et al., 2018). In this study, we utilized the GPCC-generated monthly precipitation dataset with a spatial resolution of 1°×1° from 1982 to the present (Schneider et al., 2014).

2.1.5 GRACE data

To calculate the mass balance in the study area and compare it with lake water storage changes and to investigate the contributions of the various hydrological components, in this study, we utilized the GRACE mascon products for 2002 to 2021 released by the Center for Space Research (CSR), Jet Propulsion Laboratory (JPL), and Goddard Space Flight Center (GSFC). The GRACE satellite, launched in 2002, provides monthly gravity signals resulting from surface mass redistribution, offering unprecedented spatiotemporal observation data for studying Earth's mass redistribution (Wahr et al., 1998; Tapley et al., 2019). The GRACE mascon data from the three institutions has been subjected to preprocessing, including the addition of degree one (Swenson et al., 2008) and replacement of the C20 and C30 coefficients using satellite laser ranging-based estimates (Cheng et al., 2011; Loomis et al., 2020). Additionally, to account for post-glacial rebound signals, all of the mascon products use ICE6G-D to correct for the impact of glacial isostatic adjustment (GIA) (Peltier et al., 2018). The GRACE mascon products require no further preprocessing and can be directly applied in hydrological, oceanographic, and cryospheric studies

within watersheds. Furthermore, the JPL's mascon product provides scale factors for recovering real surface signals. To address the missing months in the GRACE data and the 11-month data gap between the GRACE and GRACE-FO satellites, in this study, we employed singular spectrum analysis (SSA) to conduct data interpolation (Yi and Sneeuw, 2021).

2.1.6 Wind field data and atmospheric water vapor data

To study the physical mechanisms of the lake water level changes, in this study, we utilized the vertical wind field data ERA5 provided by the European Centre for Medium-Range Weather Forecasts (ECMWF). ERA5 is the fifth-generation reanalysis of global climate and weather data for the past 80 years, from 2002 to 2022, with a spatial resolution of 0.25°×0.25° (Hersbach et al., 2023). The atmospheric water vapor content data are based on the measurements from the ozone monitoring instrument (OMI) from January 2005 to December 2020, providing a monthly averaged total column water vapor (TCWV) dataset with a resolution of 1°×1° (Borger et al., 2021).

2.1.7 Other hydrological models

The Tianshan region contains complex hydrological components, including soil moisture, snow water, and groundwater. Therefore, land hydrological models are essential auxiliary data for studying the mass balance in the Tianshan region. The Global Land Data Assimilation System (GLDAS) is a widely used hydrological model that provides high-precision global surface land data and has been extensively used in weather and climate forecasting, water resources applications, and hydrological investigations (Bai et al., 2016; Deng and Chen, 2017). In this study, GLDAS was employed to obtain the changes in the soil moisture in the Tianshan region.

Additionally, the snow water equivalent product provided by the ECMWF was utilized to simulate the changes in the snow water in the Tianshan region. Furthermore, the WaterGAP hydrological model was employed to assess the changes in the groundwater (Müller et al., 2021).

2.2 Methods

2.2.1 Mass recovery and load vertical deformation

To obtain the time-varying gravity field information from GRACE, based on the theory proposed by Wahr et al. (1998) and using the time-variable gravity spherical harmonic coefficients ΔC_l^m and ΔS_l^m, it is possible to estimate the density anomaly at a certain point on the Earth's surface in terms of the equivalent water height:

$$\Delta EWH(\emptyset,\theta) = \frac{a\rho_e}{3\rho_W}\sum_{l=0}^{\infty}\sum_{m=0}^{l}\bar{P}_l^m(\cos\emptyset)\left(\frac{2l+1}{1+k_l}\right)[\Delta S_l^m \sin(m\theta) + \Delta C_l^m \cos(m\theta)], \quad (1)$$

where ΔEWH is the mass change expressed as the equivalent water height, $\bar{P}_l^m$ is the normalized associated Legendre polynomial, a is the Earth's radius, and ρ_e and ρ_W are the densities of the Earth and water, respectively. h_l, l_l, and k_l are the load Love numbers. Equation (1) is the fundamental equation used to calculate surface mass changes from GRACE time-variable gravity and express them in terms of the equivalent water height.

The vertical displacement of the surface mass change, Δh, can be calculated using the following formula (Fu and Freymueller, 2012):

$$\Delta h(\emptyset,\theta) = a\sum_{l=1}^{\infty}\sum_{m=0}^{l}\bar{P}_l^m(\cos\emptyset)(\frac{h_l}{1+k_l})[\Delta S_l^m \sin(m\theta) + \Delta C_l^m \cos(m\theta)]. \quad (2)$$

It should be noted that due to the certain orbital altitude of gravity satellites, the gravity field

signal attenuates with increasing altitude, making it difficult for GRACE to observe higher-degree gravity field components. Therefore, the time-variable gravity products have to be truncated at lower degree. The GRACE data has a spherical harmonic coefficient truncation at 60°, and the summation term in Equation (2) is limited to 60°. As a result, Equation (2) cannot be used to calculate the full-spectrum load displacement field. Furthermore, the GRACE time-variable gravity signal includes not only surface hydrological mass changes but also the influences of non-hydrological (tectonic) signals (Rao and Sun, 2022). When calculating the load deformation, the non-hydrological signals need to be removed. Therefore, the vertical displacement caused by the surface mass change Δm at the calculation point can be calculated using the following formula (Farrell, 1972; Erikson and MacMillan, 2014):

$$U_h = \iint \Delta m(\theta', \varphi') G_R(\alpha) \cos\varphi' d\theta' d\,\varphi', \tag{3}$$

where α is the angular distance between the load point and the load source, and $G_R(\alpha)$ is the vertical displacement Green's function, which is typically based on the preliminary reference Earth model (PREM) (Farrell, 1972).

2.2.2 Estimation of lake water storage changes

To calculate the changes in the lake water volume over a period of time, in this paper, altimetry data are utilized to obtain the lake water surface elevations and remote sensing data are utilized to obtain the lake surface areas. Furthermore, following the method proposed by Taube (2000), we can estimate the changes in the lake water volume:

$$\Delta V = \frac{1}{3}(L_2 - L_1) \times \left(S_1 + S_2 + \sqrt{S_1 S_2}\right), \tag{4}$$

where ΔV is the change in the lake water volume (km^3), L_1 and L_2 are the water levels in two

consecutive time periods, and S_1 and S_2 are the corresponding areas. Calculating the lake water storage change typically involves computing the difference between two consecutive time periods.

2.2.3 Analysis of time series

To investigate the periodic variations in the Tianshan region, Fourier transformation was utilized to analyze the periodic spectral characteristics of the various mass components. Subsequently, a least-squares method is applied to fit the time series and obtain the long-term trend and periodic components. The specific fitting method can be expressed as follows:

$$f(t) = a + bt + \sum_i A_i \cos\left(\frac{2\pi}{T_i}(t - \varphi_i)\right) + \varepsilon, \quad (5)$$

where $T_1 = 1$ is a one-year period; $T_2 = 0.5$ is a half-year period; A_i and φ_i are the amplitude and phase, respectively; and ε is the fitting residual.

2.2.4 Composition analysis

Composition analysis is the process of combining or synthesizing two different states or characteristics of meteorological variables. By calculating the sample means of both variables, it allows us to compare whether there are significant differences between the two states. The significance level is determined using t-tests:

$$t = \frac{\overline{x_1} - \overline{x_2}}{\sqrt{\frac{(n_1 - 1)s_1^2 + (n_2 - 1)s_2^2}{n_1 + n_2 - 2}}} \cdot \frac{1}{\sqrt{\frac{1}{n_1} + \frac{1}{n_2}}}, \quad (6)$$

where $\overline{x_1}$ and $\overline{x_2}$, s_1^2 and s_2^2, and n_1 and n_2 are the means, variances, and sample sizes of the two states (1 and 2), respectively. This equation follows a t-distribution, and the degrees of freedom (df) are equal to $n_1 + n_2 - 2$.

3 Results

3.1 Long-term and seasonal variations in water levels in the Tianshan lake complex

We utilized lake water level data products derived from multisource altimetry satellite data released by various institutions to obtain a time-series of the water level changes in the lake complex within the study area (Figure 2a). The trends in the water level changes of the lakes in the Tianshan region exhibited distinct characteristics, and the roles of glacier melting and anthropogenic factors cannot be overlooked in these lake level variations. Taking Lake Bosten's water level changes as an example, its water level variation differed significantly from those of the other lakes. Lake Bosten's water level has been continuously decreasing since 2002, reaching a minimum in 2014, followed by a gradual recovery after 2016. The overall water level change trend was V-shaped. This is attributed to the accelerated glacier retreat in the region after 2016 (Yi et al., 2016), which led to significant replenishment of Lake Bosten's water source. The lake's water level reached its peak around 2020 and has been declining since then. This implies that, in the long term, glacier melting could adversely impact the ecological environment around Lake Bosten. Moreover, the inconsistent characteristics of the water level changes of the different lakes primarily arise from the differences in their geographic distribution. Taking Lake Kapchagay and Lake Balkhash as examples, the Ili River provides 70–80% of the runoff from Kapchagay Lake to Lake Balkhash (de Boer et al., 2021). These lakes rely on precipitation and snowmelt for their water supply. The water storage in Kapchagay Lake affects the water level of Lake Balkhash, and changes in Kapchagay Lake's water level precede those of Lake Balkhash (red and blue solid lines in Figure 2a).

All of the lakes within the lake complex exhibit significant annual, semi-annual, and medium- to long-term periodic signals, which are manifested by the presence of approximately 6.9-year periodic signals in the frequency spectra of most of the lakes (Figure 2b). Chen et al. (2017) analyzed the strength and time-frequency characteristics of nearly 65 years of El Niño–Southern Oscillation (ENSO) events from January 1951 to May 2016, using indices such as the Oceanic Niño Index (ONI), the Southern Oscillation Index (SOI), and the multivariate ENSO index (MEI). They reported 22 warm events (El Niño) and 13 cold events (La Niña) during this period. Frequency analysis of ENSO characteristics revealed a higher occurrence of strong El Niño months compared to strong La Niña months. The ENSO cycle primarily exhibited a periodicity of 2–7 years and also exhibited a decadal variability of 10–16 years. Thus, the 6.9-year periodic signal observed in this study is consistent with the findings of Chen et al. (2017), suggesting that the underlying physical mechanism behind the lake water storage variations in the Tianshan region is fundamentally influenced by the ENSO. Additionally, Yi and Sun (2014) identified a 5-year cycle in the Pamir and Kunlun regions, while Wen et al. (2023) used longer-span data to identify a cycle of close to 6.6 years. The 6.9-year periodicity observed in our study of the lake complex seems to encompass the range of 5–7 years and is likely influenced by the Arctic Oscillation and El Niño–Southern Oscillation.

From 2002 to 2022, the long-term trend of the water level changes in the lake complex in the Tianshan region (weighted by the area of all of the lakes) was 0.01 m/a (0.73±0.10 Gt/a). Figure 2c presents the spatiotemporal distribution of the annual variations in the water levels of the individual lakes in the Tianshan region from 2002 to 2022. The change periods of the different lakes are indicated based on the month of the peak water levels. Among the eight lakes studied,

four lakes in the northeast exhibited rising water levels, with an average rate of increase of 0.06±0.001 m/a (ranging from 0.004 to 0.082 m/a). In contrast, four lakes in the southwest experienced declining water levels, with an average decrease rate of −0.006±0.00003 m/a (ranging from −0.0182 to −0.01 m/a). The seasonal variation cycle of the eight lakes in the Tianshan region shows that the peak water levels occurred in May, June, and July, but Lake Bosten's peak water level occurred in March. This spatial heterogeneity in the timing of the lake level changes highlights the variability in the lake cycles.

Importantly, there were two significant instances of anomalous water level changes in the lake complex. These occurred around 2010 and 2016. The primary sources of the water input to the Tianshan lake complex were precipitation, ice melting, and anthropogenic factors, and precipitation was the fundamental factor. By performing a singular spectrum decomposition on the time series of the water level changes for each lake and selecting the first component for differencing, the rate of change of the lake water levels was obtained (Figure 2d). The differenced lake water level changes clearly highlight the impact of increased precipitation on the lake water levels. Abnormal precipitation occurred in both the 2008–2010 and 2014–2016 periods, leading to noticeable water level anomalies across all of the lakes, albeit with distinct time lags. Notably, Lake Kapchagay (Lake 2, blue line) exhibited synchronized peaks and three periods of increased precipitation in 2010, 2013, and 2016. In contrast, Lake Zaysan (Lake 6, green line) exhibited a peak in 2013, instead of in 2016. This suggests that Lake Zaysan's water level changes were affected by anthropogenic factors and reflect the implementation of flood prevention measures. The spatiotemporal characteristics of these two instances of anomalous lake water level changes will be further analyzed in the subsequent section.

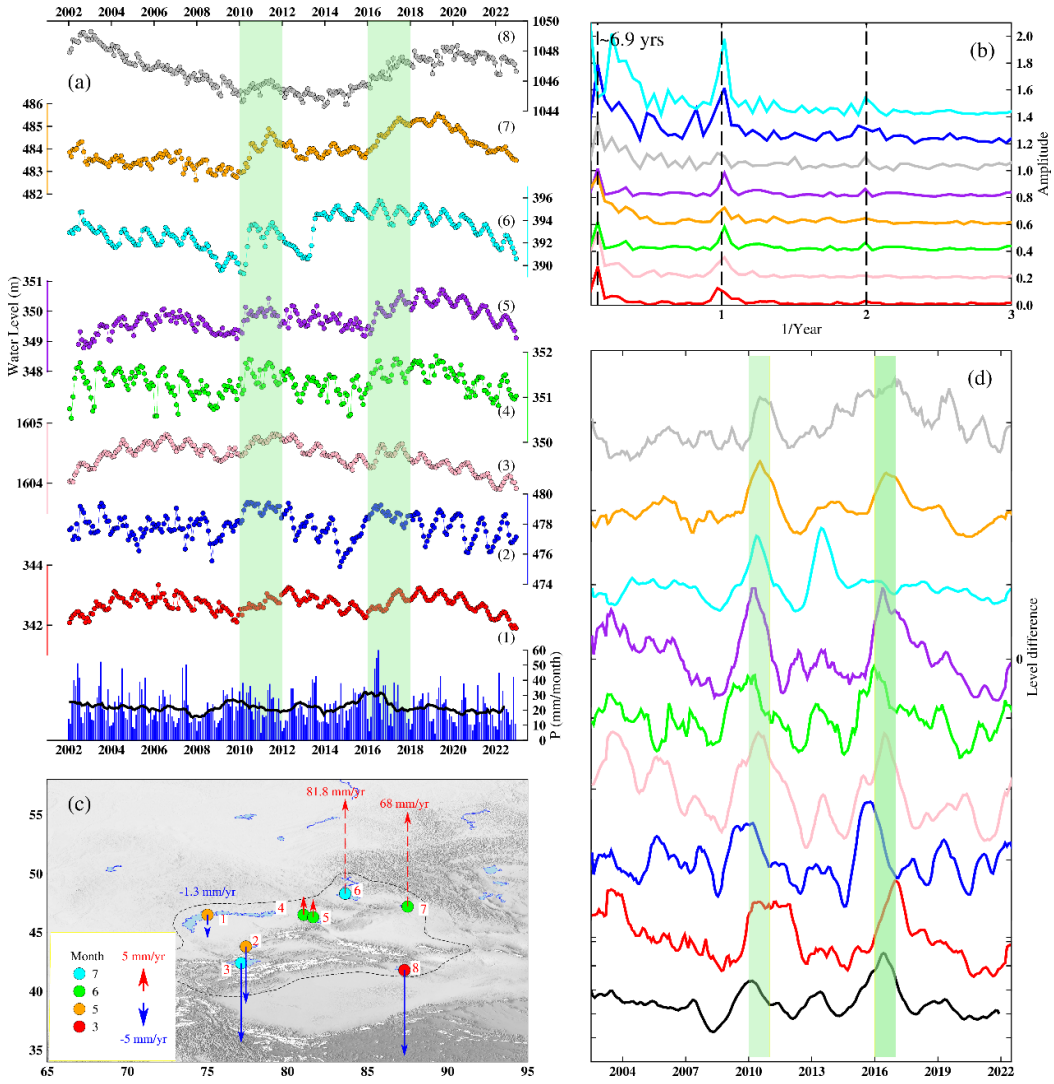

Figure 2. (a) Time series of water level changes and corresponding precipitation variations for the lake complex within the study area from 2002 to 2022. The lake numbers are the same as in Figure 1. (b) Spectral transformations of water level changes for the eight lakes. (c) Peaks in lake level variations. Spatial distribution of peaks in lake level variations in the Tianshan region and the water level change trend for each lake. The lengths of the dashed arrows are not proportional to the other lakes' water level changes. (d) Differenced lake water level changes of the first component after singular spectrum analysis (SSA) decomposition. The curves of the same color represent the same lake, and the green shaded regions denote the two anomalous periods.

In addition to the long-term trends in the lake water levels, in this study, we further investigated the seasonal trends of the lake levels. The seasonal trends capture the changes during specific months of the year within the study period (e.g., the trend for spring covers March–May each year). We divided the year into four seasons: spring (March–May), summer (June–August), autumn (September–November), and winter (December–February). Figure 3 illustrates the seasonal trends of the water levels of the individual lakes within the Tianshan region from 2002 to 2022. The seasonal interannual trends of the eight lakes in the Tianshan region exhibited similar patterns, with a rate of 0.0128±0.001 m/a in spring, 0.0141±0.001 m/a in summer, and 0.0073±0.001 m/a in autumn and winter. Furthermore, lakes Alakol, Zaysan, and Ulungur all exhibited increasing seasonal water level trends, while Lake Issyk-Kul and Lake Bosten exhibited decreasing trends. Lake Balkhash exhibited an increasing trend in summer and a decreasing trend during the other seasons, contributing to the overall long-term decreasing trend of the lake. Lake Kapchagay exhibited an increasing trend in spring and a decreasing trend in the other seasons. The water level changes of Lake Balkhash and Lake Kapchagay exhibited opposite trends in spring and summer.

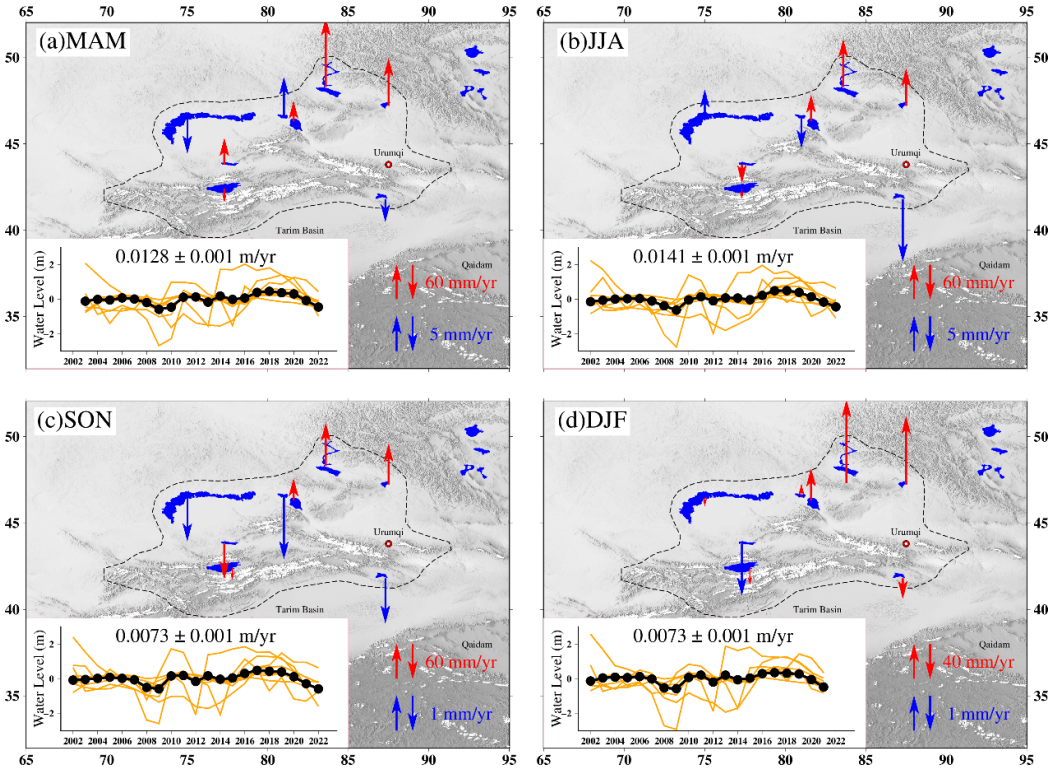

Figure 3. Spatiotemporal characteristics of the seasonal trends of the lake water levels of the lakes in the Tianshan region from 2002 to 2022: (a) Spring (MAM); (b) Summer (JJA); (c) Autumn (SON); and (d) Winter (DJF). The time series of the water-level changes for all of the lakes in each season are shown in the insets, the black line is the area-weighted lake level time series, and the numbers above the insets are the overall trends based on the area-weighted water level trends. Please note that the arrows of different colors indicate different magnitude levels.

3.2 Spatiotemporal variations in lake water storage during two anomalous periods

In the previous section, the long-term and seasonal trends of the lake water level changes in the Tianshan region were analyzed. In particular, two instances of anomalous fluctuations in water levels were identified. Lakes respond to precipitation not only through changes in water levels but also through variations in their surface areas. Using the GEE, we obtained information about the

changes in the lake surface areas in the Tianshan lake complex during the two anomalous periods. Similar to the changes in the water levels, the variations in the lake surface areas also exhibited two transition periods. During the first anomalous period, except for Lake Balkhash's contraction (decrease from 959.68 km² to 931.87 km², i.e., by 28.81 km²), the surface areas of the other lakes increased. The total lake surface area for the entire region changed an 35,230.15 km² to 35,345.55 km², i.e., an increase of 115.4 km². In the second anomalous period, the surface areas of all of the lakes increased, and the total lake area increased from 35,425.56 km² to 35,580.55 km², i.e., a total increase of 154.99 km². To further analyze the spatial changes in the lakes, Figure 4a displays subfigures that highlight the spatial patterns of the area changes for Kapchagay Lake, Zaysan Lake, and Lake Balkhash. Kapchagay Lake exhibited significant area changes from 2008 to 2010, while Zaysan Lake and Lake Balkhash exhibited evident changes during the second anomalous period. Notably, the lakes with pronounced area changes were mainly located in the low-lying areas where rivers flowed into the lakes. In addition to the clearly visible area changes during the two anomalous periods, each lake experienced maximum and minimum area values during the entire study period (Table 2). During the entire study period, from 2002 to 2021, Zaysan Lake exhibited the largest area change, reaching 779.45 km², while Sasykkol Lake exhibited the smallest change (7.57 km²). The maximum area change for each lake is presented in Table 2.

Table 2. Comparison of maximum and minimum areas of the lakes in the Tianshan lake complex from 2002 to 2021

No.	Lake name	Maximum area (km^2)	Minimum area (km^2)	Area change (km^2)
1	Balkhash	17118.95	16821.48	297.47
2	Kapchagay	1256.46	1094.31	162.15
3	Issykku	6214.51	6205.74	8.77

4	Sasykkol	754.72	747.15	7.57
5	Alakol	3097.39	2956.20	141.19
6	Zaysan	4861.01	4081.56	779.45
7	Ulungur	869.71	840.85	28.86
8	Bosten	1095.09	887.62	207.47

444

445 Estimating the variations in the lake water storage is crucial for studying the mass balance in
446 the Tianshan region. By utilizing lake water level changes obtained from altimetry data and lake
447 area changes obtained from remote sensing imagery, we established water level-area relationships
448 for each lake and then estimated the water volume changes for all of the lakes (Figure 4a). The
449 calculation results reveal that from 2003 to 2022, most of the lakes experienced two anomalous
450 periods, during which significant water volume changes occurred. At the annual scale, the
451 cumulative water volume change results (orange solid line in Figure 4a) indicate that there were
452 distinct variations during the anomalous periods. To study the overall water volume changes in the
453 entire region, in this study, we summed the water volume changes for all of the lakes. Figure 4b
454 presents the mass variations of the total water storage in the Tianshan lake complex. Two distinct
455 periods of water volume increase can be identified. During the two-year period from 2010 to 2011,
456 the total mass of the lake water mass increased by 25.07 Gt, and during the two-year period from
457 2016 to 2017, the total water mass increased by 14.66 Gt. It should be noted that after 2018, the
458 total lake water mass in the study area decreased continuously, with a reduction of greater than 10
459 Gt/a after 2020.

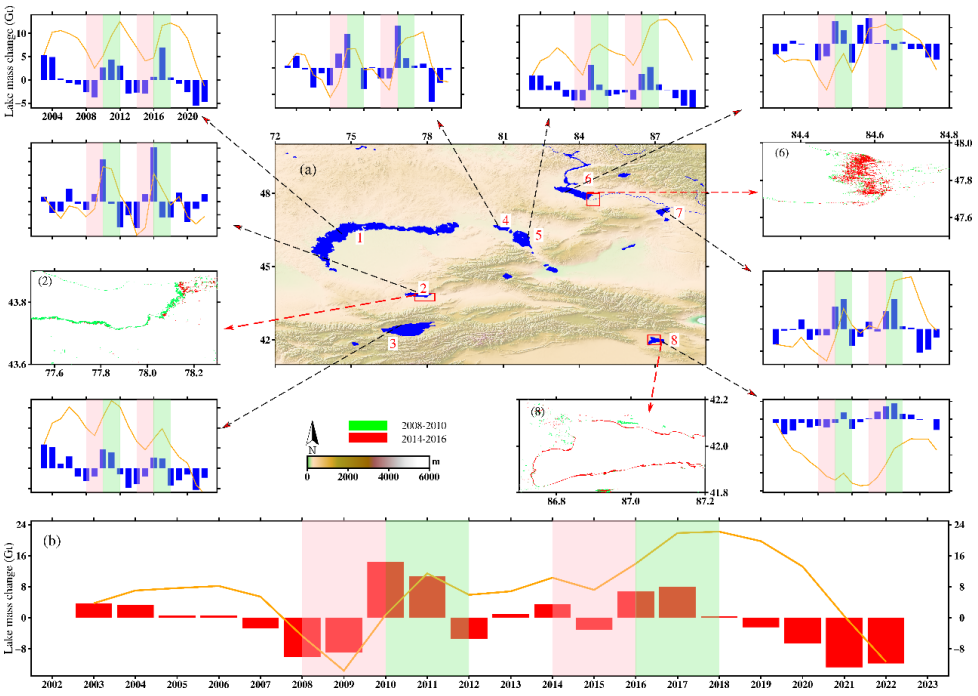

Figure 4. (a) Time series of water storage changes (blue) and cumulative water storages (orange) for the various lakes in the Tianshan region from 2002 to 2022. The lake area changes for Kapchagay Lake, Zaysan Lake, and Bosten Lake during 2008–2010 and 2014–2016 are indicated by the red arrows. (b) Time series of total water storage changes for all of the lakes in the study area. The red bars represent the annual water storage changes in the lake complex, and the orange solid line represents the cumulative change in the water storage. The pink and green shaded areas represent the dry and wet periods, respectively.

To study the impact of the anomalous lake water storage during the two anomalous periods on the regional mass balance, we obtained total mass change data for the Tianshan region from the GRACE satellite mission. Zhang et al. (2019) assessed the suitability of using GRACE mascon data for the Tianshan region and reported good agreement with GRACE spherical harmonic products across the entire area. Hence, in this study, we utilized GRACE mascon data provided by

three major institutions (CSR, JPL, and GSFC) to derive the total mass change rates for the study area from 2002 to 2021, which were −7.41±0.35 Gt/a, −7.51±0.34 Gt/a, and −9.56±0.37 Gt/a, with an average rate of change of −8.16±0.36 Gt/a. It is important to note that during the study period, these mass change results also contained two anomalous periods, which corresponded with the anomalous periods of the water level changes in the lake complex discussed earlier. During the two anomalous periods, the total mass increased by 65.73 Gt and 67.35 Gt, respectively. The changes in the lake surface area during these periods constituted merely 0.01% and 0.014% of the entire study area, but the contribution of the mass changes during the two anomalous periods accounted for 22% and 14%, respectively. This indicates that the lake water storage variations had a significant influence on the regional mass balance during the anomalous periods.

Changes in lake water storage are part of the regional mass variations and are closely connected to changes in the soil moisture, snow water, and groundwater. The characteristics of the changes in the other components will be analyzed specifically in the discussion section.

3.3 Physical mechanism behind the two anomalous periods

In the previous section, we calculated and analyzed the long-term and seasonal variations in the lake water and the variations in the two anomalous period in the Tianshan region. The occurrence of two anomalous periods in the Tianshan region, reflected by the lake water levels and area changes, was significantly influenced by the abnormal variations in the precipitation. Therefore, understanding the physical causes behind the anomalies in the precipitation is crucial. Figures 5a and 5b display the strong correlation between the annual average precipitation in the Tianshan region and the ENSO ($r=0.55$, $p<0.01$). To further analyze the connection between the

lake water storage in the two anomalous periods and precipitation, in this section, we employ a composite analysis method to delve into the physical mechanisms underlying the abnormal precipitation. Similar methodologies have also been applied to study the responses of lakes on the Qinghai–Tibet Plateau to climate (Lei et al., 2019). Figure 5c indicates that during El Niño-dominated years (1994, 1997, 2002, 2004, 2006, 2010, and 2016), the precipitation in the Tianshan region tended to increase.

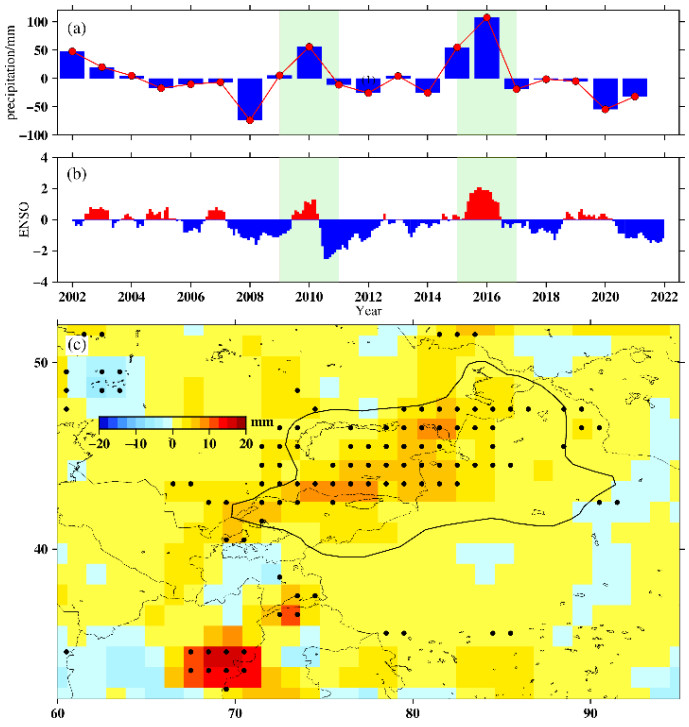

Figure 5. (a) Annual average precipitation in the Tianshan region; (b) ENSO index; (c) Precipitation anomalies during El Niño-dominated years (1994, 1997, 2002, 2004, 2006, 2010, and 2016) relative to the average climatic state from 1979 to 2021. The dotted areas indicate significant values at the 90% confidence level determined using the student's t-test.

As one of the world's largest mid-latitude arid regions, the Tianshan area is susceptible to the

508 impacts of global climate change (Zhang et al., 2022b). The occurrence of precipitation requires
509 the convergence of significant amounts of water vapor, and the distribution of the water vapor
510 affects the formation of clouds and precipitation, aerosol growth, and other phenomena, thereby
511 playing a crucial role in meteorological phenomena and climate conditions (Grossi et al., 2015).
512 We observed that the spatial distribution of the precipitation anomalies in 2010 and 2016 (Figures
513 6c, d) closely resembled the spatial distribution of the total atmospheric water vapor content
514 (Figures 6a, b). This correspondence indicates that the water vapor content in the study area
515 increased during these years, creating favorable conditions for precipitation. Notably, the water
516 levels of the lakes in the Tianshan region peaked in 2006, which was an El Niño year. To validate
517 the increase in precipitation during these years, we compared the precipitation amounts in 2006,
518 2010, and 2016 with the climatic average. Figure 6e shows that the precipitation in 2006 did not
519 pass the significance testing, suggesting that the water level increase in 2006 may have been
520 caused by other factors, such as snowmelt. In contrast, the years with two instances of anomalous
521 mass changes (2010 and 2016) exhibited more pronounced increases in precipitation compared to
522 the El Niño-dominated years (1994, 1997, 2002, 2004, 2006, 2010, and 2016) (Figure 5c), with
523 significance demonstrated at the 90% confidence level (Figures 6c, d). Furthermore, during the
524 anomalous periods in 2010 and 2016, the vertical wind field intensity at 500 hPa also exhibited
525 enhancement along the Tianshan mountain range (Figure 6f). This intensified vertical motion
526 facilitated the convergence of more water vapor in the study area, leading to increased
527 precipitation. Consequently, the Tianshan region experienced two significant mass anomalies in
528 2010 and 2016 due to these pronounced shifts in precipitation.

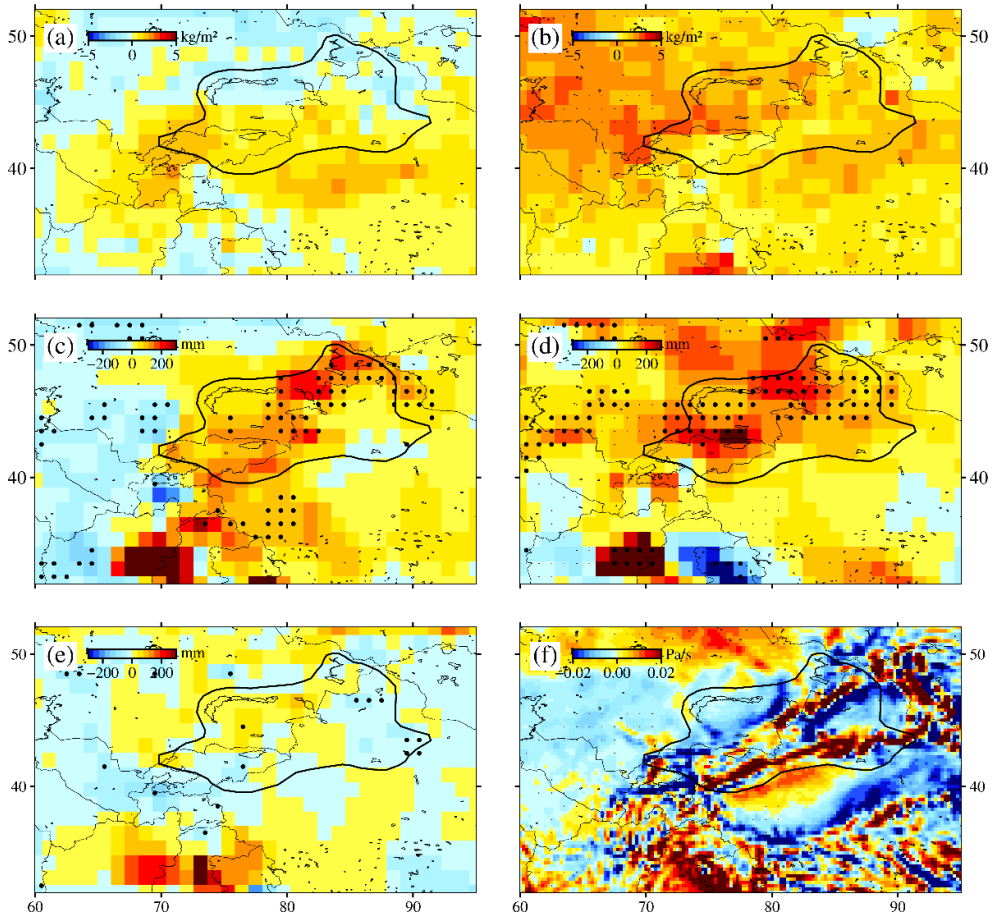

Figure 6. Distribution of atmospheric total water vapor anomalies during the two anomalous mass change periods in the study area: (a) 2010 and (b) 2016. Anomalies in average precipitation in (c) 2010 and (d) 2016. (e) Anomalies in average precipitation in 2006; (f) Anomalies in the 500-hPa vertical wind field during the two El Niño years: 2010 and 2016. The dotted areas indicate significant values at the 90% confidence level determined using the student's t-test.

4 Discussion

In this study, multisource remote sensing observations were utilized to investigate the water storage changes in the lake complex in the Tianshan region in China. Building upon the computation and analysis of the spatiotemporal distribution characteristics of the water storage changes in the lake complex, we identified two major anomalous periods (2010 and 2016).

Considering the presence of various other hydrological components in the Tianshan region, further discussion is warranted regarding the spatiotemporal distribution characteristics of the quality changes in the different hydrological components, their variations during the two anomalous periods, and the resulting load deformation effects on the surface GNSS observations.

4.1 Characteristics of changes in various hydrological components and their relationship with lake water storage variations

The total mass changes in the Tianshan region were highly complex, and the variations in the lake water storage represent only one facet of the hydrological changes in the surrounding area. These variations were closely related to other hydrological components such as glaciers, soil moisture, groundwater, and the snowmelt equivalent. However, it remains unclear to what extent each hydrological component contributed to the changes in the lake water storage, that is, what proportion of the total mass changes each component accounted for in the study area. This warrants further exploration and analysis. To address this, we initially employed GRACE satellite gravity data to deduce the overall mass changes across the study area. Then, by utilizing a range of remote sensing observations and hydrological models to separate individual hydrological components, we analyzed the contribution of each component to the variations in the lake water storage within the context of the regional mass changes. The variations in each hydrological component encompassed long-term trends and periodic fluctuations. Once these variations were effectively isolated, further research and analysis could be conducted to delve into the characteristics of the changes in each hydrological component during the two anomalous periods of lake water fluctuations.

Using the data provided by Barandun et al. (2020) and Hugonnet et al. (2021), we calculated

562 the glacier melting rates in each sub-region of the Tianshan region (Figure 7). The results indicate
563 that significant glacier mass loss occurred. Furthermore, the results show that the glacier melting
564 time series of Barandun et al. (2020) and Hugonnet et al. (2021) for the western Tianshan and
565 eastern Tianshan regions were consistent, while in the central Tianshan, Barandun et al. (2020)
566 estimated a slightly faster glacier melting rate. Barandun et al. (2020) estimated the annual glacier
567 melting rate in the Tianshan region to be −3.78 Gt/a from 2000 to 2018. Hugonnet et al. (2021)
568 estimated the glacier mass change time series for the Tianshan region and obtained a glacier
569 melting rate of −3.53 Gt/a from 2000 to 2021, which is close to the trend derived by Yi et al.
570 (2016) using ICESat data (−3.4 Gt/a). The two estimated glacier melting rates are quite consistent.
571 However, considering the periodic variations in the glaciers, in this study, we selected the glacier
572 change results of Hugonnet et al. (2021) for use in the subsequent research analysis.
573

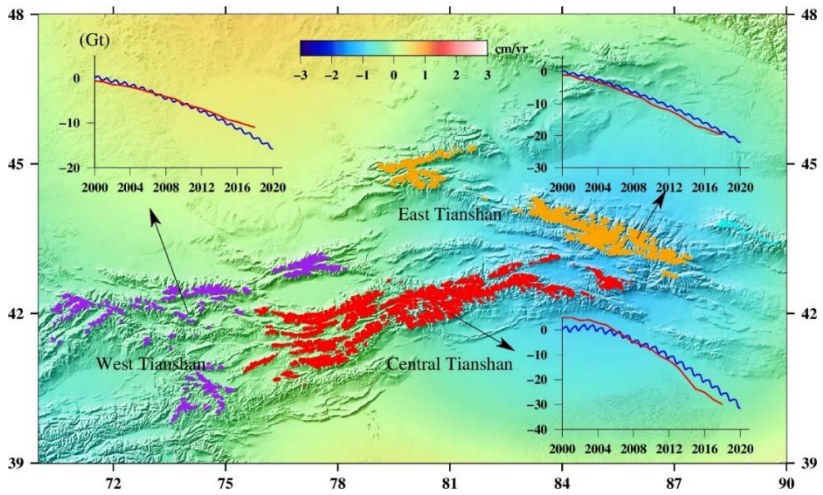

574

575 **Figure 7**. Cumulative glacier change time series for the western, central, and eastern sub-regions of the Tianshan
576 region calculated using the data provided by Barandun et al. (2020) and Hugonnet et al. (2021). The background
577 shows the long-term trend of the mass changes in the Tianshan region obtained using GRACE data.
578

579 In addition, we considered the changes in the soil moisture, canopy, snow water equivalent,
580 and groundwater. We used the GLDAS Noah hydrological model to calculate the soil moisture
581 changes in the Tianshan region. The results indicate a long-term increasing trend with a rate of
582 0.46±0.25 Gt/a. The changes in the canopy and its long-term trend were both close to zero, so the
583 effect of the canopy was neglected in this study. Furthermore, we extracted the trend of the snow
584 water equivalent (−0.06±0.11 Gt/a) from the ECMWF model, and the groundwater change rate
585 (−0.08±0.04 Gt/a) from the WGHM model. The time series of the mass changes for these
586 hydrological components after being subjected to a 1-year moving average are presented in Figure
587 8a. The results show that all of the hydrological components exhibited two periods of exceptional
588 fluctuations. These periods were consistent with the anomalous periods of lake water level
589 variations. The long-term trends of the snow water, groundwater, and glaciers were continuous
590 decreasing trends, while the soil moisture and lake water exhibited increasing trends. Based on
591 these findings, we infer that the ongoing melting of the glaciers in the Tianshan region contributed
592 to the increases in the lake water and soil moisture.

593 Regarding the long-term trends of the various hydrological components, the glacier melting
594 exhibited a significant rate of change, while the trends of the other hydrological components were
595 almost stable. Table 3 presents the long-term trends, annual amplitudes, and phases of the changes
596 in the hydrological components. The results show that the contribution of the lake water storage
597 changes to the total GRACE signal was negligible. Among the components, the glaciers exhibited
598 the largest rate of decrease, while the mass changes of the other hydrological components were
599 relatively stable. In particular, the two periods of exceptional fluctuations better reflect the impact
600 of each hydrological component on the overall mass balance in the Tianshan region. Although the

trend of the lake water changes was small, its contributions during the two anomalous periods were 22% and 14%, respectively, indicating significant increases in its contribution. The soil moisture and snow water signals predominantly contributed during the first period of change, accounting for 93.98% and 14.67%, respectively. During the second anomalous period, the contributions of the soil moisture and snow water were 69.25% and 20.83% (Figures 8b, c). During the two periods of mass anomalies, the soil moisture contributed significantly, while the changes in the snow and lake water made comparable contributions.

Figure 8d presents the interannual mass changes of each hydrological component. The snow water accumulated during the winter and spring and reached its peak in March. As temperature increased in summer, the snow gradually melted, and the soil moisture reached its peak in May, while the groundwater and lake water reached their peaks in July. In addition, the annual amplitudes of the snow water and soil moisture contributed significantly to the annual amplitude of the GRACE signal. This suggests that the total annual mass changes observed in the study area by GRACE were mainly driven by the snowmelt and the annual fluctuations in the soil moisture.

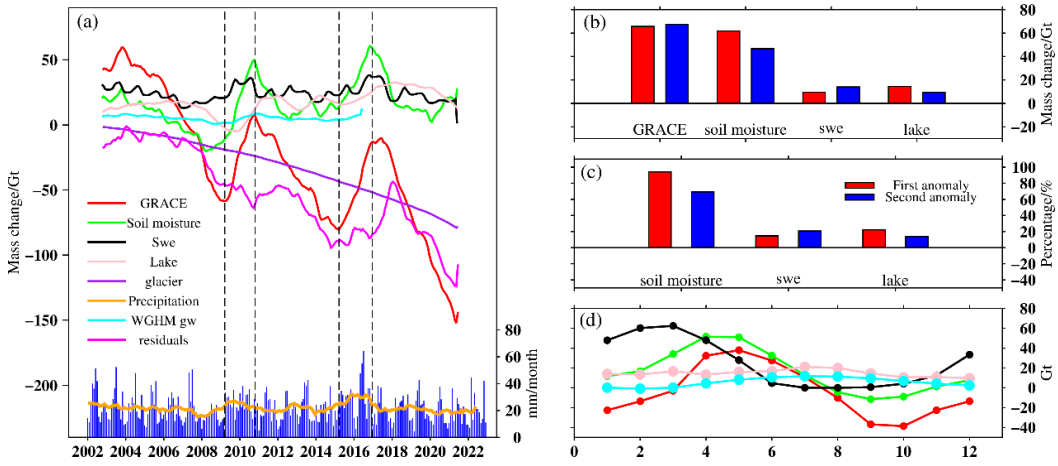

Figure 8. Mass change time series of the various hydrological components from 2002 to 2021: (a) Smoothed mass

618 change time series of each component. The dashed lines represent the mass differences during the two mass
619 anomaly periods from 2008 to 2010 and from 2014 to 2016. (b) The total mass and the increase in mass of each
620 hydrological component during the two mass anomaly periods. (c) The percentage contribution of each
621 hydrological component to the total mass increase during the two mass anomaly periods. (d) The intra-annual mass
622 variations of each hydrological component in the study area.

623

624 Table 3 Mass change rate of each hydrological component within the study area

Mass component	Annual amplitude (Gt)	Phase (days)	Trend (Gt/a)	Mass change during the first anomaly (Gt)	Mass change during the second anomaly (Gt)
GRACE	32.87	98.60	−8.16±0.36	65.73	67.35
Soil moisture	10.56	94.53	0.46±0.25	61.77	46.64
lake	5.24	168.69	0.73±0.10	14.54	9.36
snow	31.71	36.95	−0.06±0.11	9.64	14.03
glacier	-	-	−3.53	-	-
groundwater	5.61	197.4	−0.08±0.04	6.82	-
-: No data					

625

626 The spatial distributions of the precipitation, total mass changes monitored by GRACE, soil
627 moisture, and snow water equivalent during the two anomalous mass change periods are presented
628 in Figure 9. The spatial distribution of each hydrological component during these periods reflects
629 the geographic variation in the precipitation. During the first anomalous mass change period, the
630 largest total mass changes occurred in the western Tianshan region and the northern part of the
631 study area, forming a strip-like pattern along the Tianshan Mountains. In contrast, during the
632 second transition period, the mass increases were mainly concentrated in the lake region. The

633 spatial distribution of the mass increased during both anomalous periods (Figures 9c, d) and
634 closely corresponded to the spatial distribution of the increase in precipitation (Figures 9a, b),
635 suggesting that the increased precipitation led to a corresponding increase in the soil moisture,
636 resulting in an overall mass increase across the study area. By comparing the spatial distributions
637 of the soil moisture (Figures 9e, f) and the snow water equivalent (Figures 9g, h), we found that
638 the areas with increased soil moisture were primarily located within the lake region. By comparing
639 the changes in the snow water and lake water shown in Figure 8a, we inferred that the interannual
640 lake water level changes were not solely driven by direct rainfall. With increasing temperature, the
641 accumulated snow began to melt and slowly infiltrated into the soil, leading to an increase in the
642 soil moisture. The increase in the soil moisture was subject to a certain time delay in response to
643 the changes in the snow water. Liu et al. (2022) reported that a substantial amount of rainfall
644 needs time to saturate the soil after falling and subsequently enters the lakes via surface runoff.
645 Hence, the peak water levels of the lakes occurred during the troughs of the snow water
646 distribution.

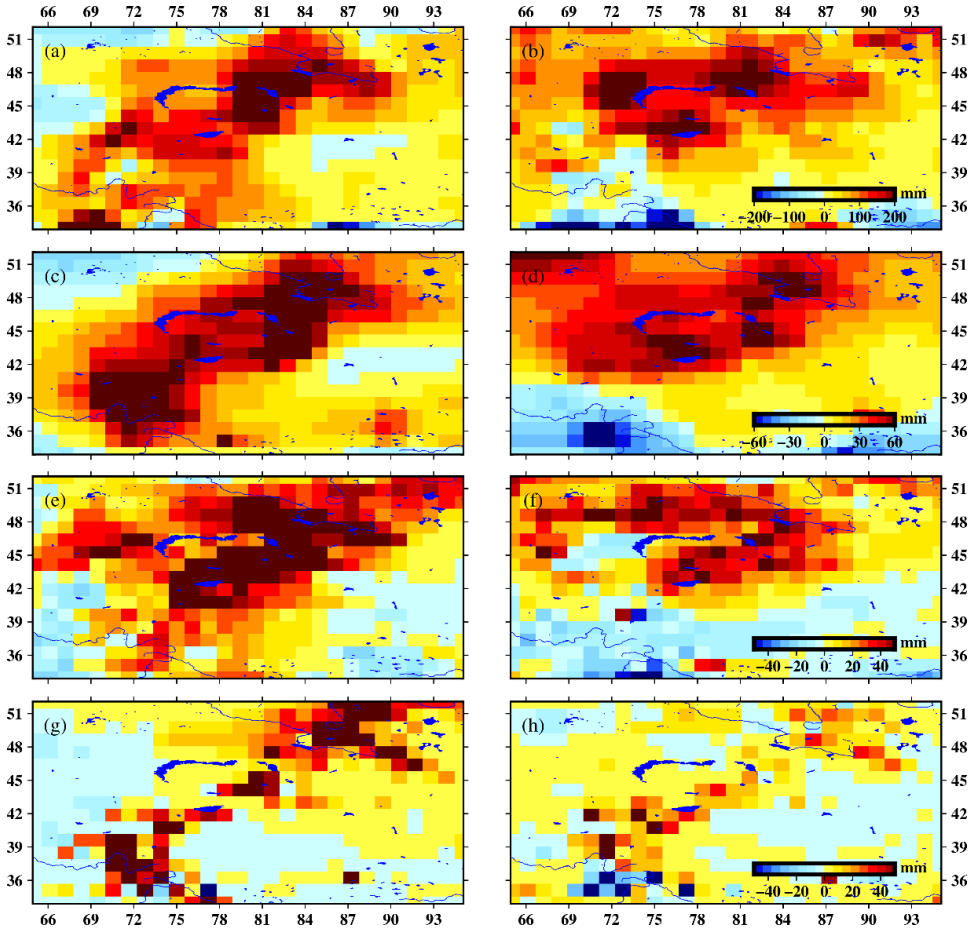

Figure 9. Spatial distribution of the changes in precipitation (a, b), the total hydrological mass changes observed by GRACE (c, d), the soil moisture (e, f), and the snow water equivalent (g, h) during the two anomalous mass change periods within the study area. The left column (a, c, e, g) corresponds to the first anomalous mass change period in 2010, while the right column (b, d, f, h) corresponds to the second anomalous mass change period in 2016.

4.2 Load correction and its impact on GNSS observations

The aforementioned changes in the lake complex and the various hydrological components, as well as the two instances of precipitation anomalies, were invariably associated with the significant mass anomalies, which were evident in the time-variable gravity signals inferred from

GRACE. These mass change signals undeniably induced surface loading effects on the solid Earth's surface, which should also be reflected in the surface displacement field. To verify whether this signal was captured in the vertical displacements monitored via a GNSS, we employed GNSS data provided by the Nevada Geodetic Laboratory (http://geodesy.unr.edu/NGLStationPages/stations/) to calculate the surface displacements. Due to the temporal coverage of the GNSS data, we selected GNSS stations with time series that encompassed the mass anomaly periods. To derive the vertical displacements induced by the surface mass changes, we removed the contributions of the global atmospheric loading and non-tidal ocean loading effects from the vertical displacements at these GNSS stations. The resulting residual signals were then used to analyze the surface mass changes. We employed the empirical mode decomposition (EMD) method to filter and smooth the GNSS signals (He et al., 2020). After corrections for atmospheric and non-tidal ocean loading effects, the selected GNSS stations provided time series that clearly exhibited changes in the vertical surface displacements due to the mass anomalies during the two wet-to-dry transition periods (left column in Figure 10). The results show that during the first mass anomaly period in 2010, GNSS station SELE exhibited a significant jump in the vertical displacement, while stations CHUM and TALA exhibited downward trends during both mass anomaly periods. This suggests that the magnitudes of the mass changes generated by the two mass anomalies were sufficient to induce noticeable surface deformations that could be detected by the GNSS.

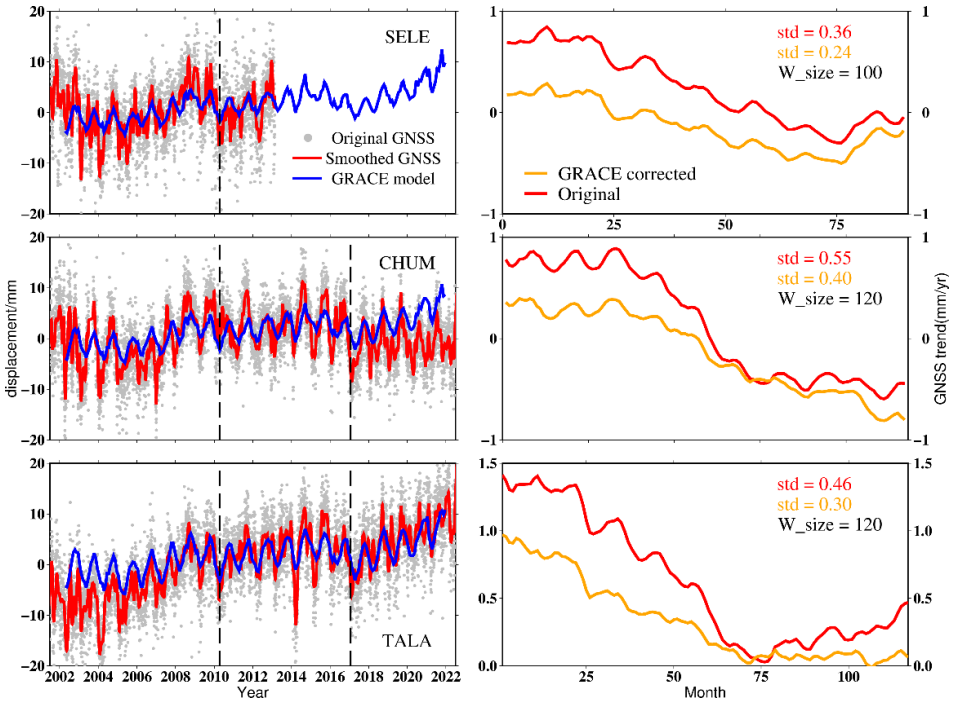

678

679 **Figure 10**. Time series of vertical displacements at GNSS stations in the Tianshan region (left column) and the

680 changes in the sliding trends at the corresponding stations (right column). The sliding long-term trends have been

681 corrected for the vertical displacement due to the loading effects obtained by integrating GRACE mascon data with

682 Green's functions.

683

684 When analyzing the impact of the surface mass changes on the GNSS displacement field,

685 scientists often calculate the loading effect of the surface mass migration rate on the GNSS

686 displacement field (Rao and Sun, 2022; Wen et al., 2023). However, constructing a surface mass

687 change model is an extremely challenging task as it requires considering solid crustal

688 displacement, the mass migration associated with surface erosion/deposition, and more accurate

689 hydrological models (especially for groundwater). Since we focused solely on the surface mass

690 migration, particularly the two anomalous mass changes and their impacts on the GNSS

691 displacement field, in this study, we selected the GRACE mascon data as the global mass change

692 model and used the Green's function integration method to calculate the vertical displacement
693 caused by these loads at the three GNSS stations in order to explore the effect of correcting the
694 surface mass changes on the GNSS vertical displacements. By considering the time span of the
695 GNSS time series at each station, we then selected 100 months, 120 months, and 120 months of
696 GNSS time series for the SELE, CHUM, and TALA stations, respectively. We applied a moving
697 window with a monthly step to calculate and correct the loading vertical displacements. As a
698 result, we obtained the long-term trend of the displacement variations at the GNSS stations with
699 the sliding window changes (right column in Figure 10). The results presented in Figure 10 show
700 that after the loading correction, the stability of the vertical displacement trend variations at the
701 three stations (CHUM, SELE, and TALA) were all improved. Specifically, the standard deviation
702 of the sliding trend at CHUM, SELE, and TALA stations decreased by 33%, 27%, and 35%,
703 respectively. This indicates that the surface mass changes had a non-negligible impact on the
704 GNSS displacement field. After correcting for the mass change loading, the true crustal
705 displacement field was restored and was represented more accurately. Therefore, when studying
706 regional tectonic movements, it is essential to perform surface mass loading corrections.
707
708 **4.3 Error Analysis of Mass Balance in the Tianshan Region**
709 It is important to note that in Section 4.1, the calculated GRACE total mass change did not
710 perfectly match the sum of the contributions of the various hydrological components, indicating
711 that there were some uncertainties in the mass changes calculations for each hydrological
712 component. To investigate the sources of these uncertainties, we truncated the GRACE mascon
713 data and the multisource land surface mass change rate model to 60° and applied Gaussian 300 km

714 filtering and P4M6 decorrelation filtering. By comparing Figures 11a and 11b, it can be seen that
715 both the GRACE data and the land surface model agree well in the central and western Tianshan
716 regions, but there are significant discrepancies in the eastern Tianshan region (Figure 11c). The
717 reasons for these discrepancies are rather complex. Upon careful analysis, we found that the
718 regions with residual signals in Figure 11c contain densely distributed cities and also include oil
719 and gas extraction areas (such as the Karamay oilfield). Therefore, the groundwater in these
720 regions may experience significant depletion, and the current hydrological models are believed to
721 severely underestimate the changes in the groundwater (Döll et al., 2012; Scanlon et al., 2019),
722 which could be one of the uncertainties. Furthermore, the problem of solid mass migration in the
723 Tianshan region is highly complex (Rao and Sun, 2022; Wen et al., 2023), and research on factors
724 such as erosion, sedimentation, and crustal movement needs to be further improved and refined. In
725 conclusion, the various hydrological models used in this study contain significant uncertainties.
726 Future research on regional mass balance will rely on continually refining hydrological and
727 surface solid mass models.
728

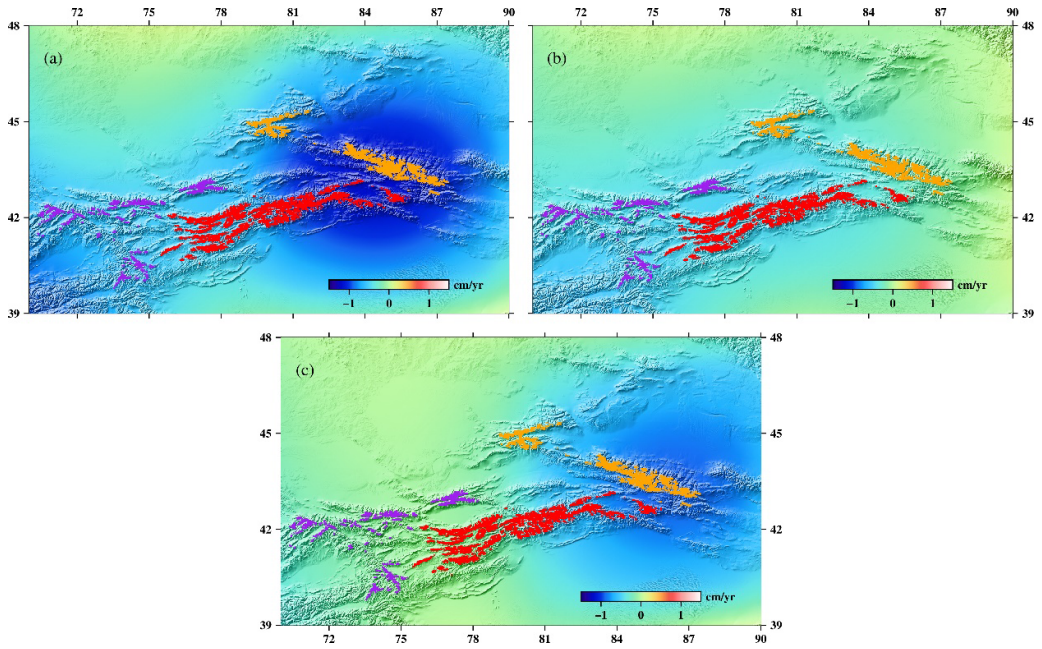

Figure 11. (a) Mass change rate in the Tianshan region obtained by truncating and filtering the GRACE mascon data; (b) Land surface mass change rate model truncated to 60° and processed using the same filters as GRACE; and (c) Difference between the truncated and filtered GRACE mascon data and the land surface mass change rate model.

5 Conclusions

In this study, we utilized multiple remote sensing datasets and hydrological models to investigate the spatiotemporal distribution characteristics of the lake water storage changes in the Tianshan region from 2002 to 2022. Two significant periods of water storage anomalies were identified during the study period. Additionally, we analyzed and calculated the contributions and proportions of the various hydrological components in the study area, and we discussed the influencing factors and physical mechanisms behind these hydrological changes. The main conclusions of this study are as follows.

The results of this study revealed that the lake water storage in the Tianshan region exhibited

744 a long-term increasing trend with a rate of 0.73±0.10 Gt/a. We also identified two periods of water
745 storage anomalies during 2008–2010 and 2014–2016. The results indicate that all of the lakes
746 exhibited significant annual and semi-annual periodic variations, as well as medium- to long-term
747 signals of approximately around 6.9 years, while Zaysan Lake exhibited a 4.1-year periodicity,
748 which was possibly due to the influence of anthropogenic factors. The 6.9-year periodic signal
749 was associated with the melting of ice and snow, which was influenced by the Arctic Oscillation
750 and El Niño–Southern Oscillation. The seasonal interannual trends of the lake complex in the
751 Tianshan region exhibited similar patterns, with rates of 0.0128±0.001 m/a in spring,
752 0.0141±0.001 m/a in summer, and 0.0073±0.001 m/a in autumn and winter. In addition, during the
753 two-year periods of 2010–2011 and 2016–2017, the total lake water storage in the Tianshan region
754 increased by 25.07 Gt and 14.66 Gt, respectively. However, after 2017, the total lake water storage
755 in the study area began to decrease continuously, with annual reductions of over 10 Gt in 2020 and
756 2021. This trend requires further observation and investigation.

757 In addition, the contributions and proportions of the various hydrological components in the
758 GRACE signal were calculated and separated. The results revealed that the soil moisture, snow
759 water equivalent, lake water, and vertical displacements observed by the GNSS all reflected the
760 two mass change anomalies. During the two anomalous periods, the changes in the lake area
761 accounted for only 0.01% and 0.014% of the total area, but the contributions of the lake water
762 increased significantly, by 22% and 14%, respectively. The contributions of the soil moisture and
763 snow water during the first anomalous period were 93.98% and 14.67%, respectively, while their
764 contributions during the second anomalous period were 69.25% and 20.83%, respectively. During
765 the two anomalous periods, the soil moisture was the primary contributor, and the snow changes

and lake water storage made roughly equal contributions. The annual water level changes in the lake complex were not only directly affected by rainfall but also significantly influenced by ice and snow meltwater.

We also identified a close correlation between the two mass change anomaly periods and the ENSO events ($r=0.55$, $p<0.01$). During El Niño–dominated years, the atmospheric water vapor content in the Tianshan region generally increased, leading to corresponding increases in precipitation. In the two anomaly years (2010 and 2016), the increase in precipitation was even more pronounced, and the vertical wind field was strengthened. These conditions led to more water vapor descending and converging in the study area, providing favorable conditions for precipitation and resulting in the occurrence of the two mass change anomalies.

By considering the lake water storage changes in conjunction with the other hydrological components, this study provides a new perspective for investigation of the mass balance in the Tianshan region. The research results highlight the need to focus on the impact of extreme climate events on the regional mass balance in the context of global climate change.

CRediT authorship contribution statement

Zhiqiang Wen: Conceptualization, Data curation, Formal analysis, Writing – original draft. **Wenke Sun**: Conceptualization, Funding acquisition, Writing – review & editing. **Shuang Yi**: Conceptualization, Funding acquisition, Investigation, Writing – review & editing.

Declaration of competing interest

The authors declare that they have no known competing financial interests or personal

relationships that could have appeared to influence the work reported in this paper.

Data Availability Statement

GNSS data：http://geodesy.unr.edu/NGLStationPages/stations/; **Lake level data**：https://nsidc.org/data/icesat-2/products, https://eocat.esa.int/sec/#data-services-area, http://hydrolare.net/catalogue.php. **GPCC Precipitation**：https://opendata.dwd.de/climate_environment/GPCC/html/download_gate.html **Wind field data**：https://cds.climate.copernicus.eu/cdsapp#!/dataset/reanalysis-era5-pressure-levels?tab=overview **Atmospheric water vapor data**：https://doi.org/10.5281/zenodo.5776718. **Groundwater datasets**: https://doi.pangaea.de/10.1594/PANGAEA.918447

Acknowledgments

This study was supported by grants from the National Natural Science Foundation of China (grant numbers 42174097, 41974093, and E3ER0402A2) and the University of Chinese Academy of Sciences Research Start-up Grant (110400M003). We thank NASA for providing GLDAS (https://ldas.gsfc.nasa.gov/gldas/), GRACE/GRACE-FO Mascon data are available at http://grace.jpl.nasa.gov, http://www2.csr.utexas.edu/grace and https://earth.gsfc.nasa.gov/geo/data/grace-mascons

References

Adrian, R., O'Reilly, C. M., Zagarese, H., Baines, S. B., Hessen, D. O.,Keller, W., Livingstone, D. M., Sommaruga, R., Straile, D., VanDonk, E., Weyhenmeyer, G. A., and Winder, M. (2009). Lakes

assentinels of climate change. Limnology and Oceanography, 54(6), 2283–2297.

Bai, P., Liu, X., Yang, T., Liang, K., and Liu, C. (2016). Evaluation of streamflow simulation results of land surface models in GLDAS on the Tibetan plateau. Journal of Geophysical Research: Atmospheres, 121(20), 12-180.

Barandun, M., Pohl, E., Naegeli, K., McNabb, R., Huss, M., Berthier, E., et al. (2021). Hot spots of glacier mass balance variability in Central Asia. Geophysical Research Letters, 48, e2020GL092084.

Borger, C., Beirle, S., and Wagner, T. (2021). A 16-year global climate data record of total column water vapour generated from OMI observations in the visible blue spectral range. Earth System Science Data Discussions, 1-25.

Brun, F., Berthier, E., Wagnon, P., Kääb, A., and Treichler, D. (2017). A spatially resolved estimate of high mountain Asia glacier mass balances from 2000 to 2016. Nature Geoscience, 10(9), 668–673.

Chen, H., Xu, F., Li, X., Xia, T., Zhang Y. (2017). Intensities and time-frequency variability of enso in the last 65 years. Journal of Tropical Meteorology, 33(5): 683-694.

Cheng, M., Ries, J. C., and Tapley, B. D. (2011). Variations of the Earth's figure axis from satellite laser ranging and GRACE. Journal of Geophysical Research, 116, B01409.

Deng, H., and Chen, Y. (2017). Influences of recent climate change and human activities on water storage variations in Central Asia. Journal of Hydrology, 544, 46-57.

de Boer, T., Paltan, H., Sternberg, T., and Wheeler, K. (2021). Evaluating vulnerability of Central Asian water resources under uncertain climate and development conditions: The case of the Ili-Balkhash Basin. Water, 13(5), 615

Döll, P., Hoffmann-Dobrev, H., Portmann, F. T., Siebert, S., Eicker, A., Rodell, M., ... and Scanlon, B. R. (2012). Impact of water withdrawals from groundwater and surface water on continental water storage variations. Journal of Geodynamics, 59, 143-156.

Farinotti, D., Longuevergne, L., Moholdt, G., Duethmann, D., Mölg, T., Bolch, T., et al. (2015). Substantial glacier mass loss in the Tien Shan over the past 50 years. Nature Geoscience, 8(9), 716–722.

Gardelle, J., Berthier, E., and Arnaud, Y. (2012). Slight mass gain of Karakoram glaciers in the early twenty-first century. Nature Geoscience, 5(5), 322-325.

Gardelle, J., Berthier, E., Arnaud, Y., and Kääb, A. (2013). Region-wide glacier mass balances over the Pamir-Karakoram-Himalaya during 1999–2011. The Cryosphere, 7(4), 1263-1286.

Grant, L., Vanderkelen, I., Gudmundsson, L., Tan, Z., Perroud, M., Stepanenko, V. M., ... and Thiery, W. (2021). Attribution of global lake systems change to anthropogenic forcing. Nature Geoscience, 14(11), 849-854.

Grossi, M., Valks, P., Loyola, D., Aberle, B., Slijkhuis, S., Wagner, T., Beirle, S., and Lang, R. (2015). Total column water vapour measurements from GOME-2 MetOp-A and MetOp-B, Atmospheric Measurement Techniques, 8, 1111–1133.

He, X., Yu, K., Montillet, J. P., Xiong, C., Lu, T., Zhou, S., ... and Ming, F. (2020). GNSS-TS-NRS: An Open-source MATLAB-Based GNSS time series noise reduction software. Remote Sensing, 12(21), 3532.

Hersbach, H., Bell, B., Berrisford, P., Biavati, G., Horányi, A., Muñoz Sabater, J., Nicolas, J., Peubey, C., Radu, R., Rozum, I., Schepers, D., Simmons, A., Soci, C., Dee, D., Thépaut, J-N. (2023): ERA5 hourly data on pressure levels from 1940 to present. Copernicus Climate Change

Service (C3S) Climate Data Store (CDS)(Accessed on 30-Apr-2023).

Heki, K. (2004). Dense GPS Array as a New Sensor of Seasonal Changes of Surface Loads. Geophysical Monograph Series.

Heki, K., and Arief, S. (2022). Crustal response to heavy rains in Southwest Japan 2017-2020. Earth and Planetary Science Letters, 578, 117325.

Hu, Z., Zhou, Q., Chen, X., Li, J., Li, Q., Chen, D., et al. (2018). Evaluation of Three Global Gridded Precipitation Data Sets in central Asia Based on Rain Gauge Observations. International Journal of Climatology, 38 (9), 3475–3493.

Hugonnet, R., McNabb, R., Berthier, E., Menounos, B., Nuth, C., Girod, L., Farinotti, D., Huss, M., Dussaillant, I., Brun, F. and Kääb, A. (2021). Accelerated global glacier mass loss in the early twenty-first century - Dataset.. [Dataset]. Theia.

Jacob, T., Wahr, J., Pfeffer, W. T., and Swenson, S. (2012). Recent contributions of glaciers and ice caps to sea level rise. Nature, 482(7386), 514-518.

Jean-Francois P., Andrew C., Noel G., Alan S. B. (2016). High-resolution mapping of global surface water and its long-term changes. Nature, 540, 418-422.

Jiang, L., Nielsen, K., Andersen, O. B., and Bauer-Gottwein, P. (2017). Monitoring recent lake level variations on the Tibetan Plateau using CryoSat-2 SARIn mode data. Journal of Hydrology, 544, 109-124.

Kääb, A., Berthier, E., Nuth, C., Gardelle, J., and Arnaud, Y. (2012). Contrasting patterns of early twenty-first-century glacier mass change in the Himalayas. Nature, 488(7412), 495-498.

Kääb, A., Treichler, D., Nuth, C., and Berthier, E. (2015). Contending estimates of 2003–2008 glacier mass balance over the Pamir–Karakoram–Himalaya. Cryosphere, 9(2), 557-564.

876 Lei, Y., Zhu, Y., Wang, B., Yao, T., Yang, K., Zhang, X., ... and Ma, N. (2019). Extreme lake level
877 changes on the Tibetan Plateau associated with the 2015/2016 El Niño. Geophysical Research
878 Letters, 46(11), 5889-5898.
879 Li, W., Chen, Y., Yuan, X., Xiao, W., and Windley, B. F. (2022). Intracontinental deformation of the
880 Tianshan Orogen in response to India-Asia collision. Nature Communications, 13(1), 3738.
881 Li, Y. A., Tan, Y., Jiang, F. Q., Wang, Y. J., and Hu, R. J. (2003). Study on hydrological features of the
882 Kaidu River and the Bosten Lake in the second half of 20th century. Journal of Glaciology and
883 Geocryology, 25(2), 215-218.
884 Liu, C., Hu, R., Wang, Y., Lin, H., Zeng, H., Wu, D., ... and Shao, C. (2022). Monitoring water level
885 and volume changes of lakes and reservoirs in the Yellow River Basin using ICESat-2 laser
886 altimetry and Google Earth Engine. Journal of Hydro-environment Research, 44, 53-64.
887 Liu, H., Chen, Y., Ye, Z. et al. (2019). Recent Lake Area Changes in Central Asia. Scientific Reports,
888 9(1): 16277.
889 Loomis, B. D., Rachlin, K. E., Wiese, D. N., Landerer, F. W., and Luthcke, S. B. (2020). Replacing
890 GRACE/GRACE-FO with satellite laser ranging: Impacts on Antarctic Ice Sheet mass change.
891 Geophysical Research Letters, 47(3), e2019GL085488.
892 Matsuo, K., and Heki, K. (2010). Time-variable ice loss in Asian high mountains from satellite
893 gravimetry. Earth and Planetary Science Letters, 290(1-2), 30-36.
894 Müller Schmied, H., Cáceres, D., Eisner, S., Flörke, M., Herbert, C., Niemann, C., ... and Döll, P.
895 (2021). The global water resources and use model WaterGAP v2. 2d: Model description and
896 evaluation. Geoscientific Model Development, 14(2), 1037-1079.
897 Olthof, I., Fraser, R. H., and Schmitt, C. (2015). Landsat-based mapping of thermokarst lake dynamics

on the Tuktoyaktuk Coastal Plain, Northwest Territories, Canada since 1985. Remote Sensing of Environment, 168, 194-204.

Pan, Y., Chen, R., Yi, S., Wang, W., Ding, H., Shen, W., and Chen, L. (2019). Contemporary mountain-building of the Tianshan and its relevance to geodynamics constrained by integrating GPS and GRACE measurements. Journal of Geophysical Research: Solid Earth, 124(11), 12171-12188.

Pan, Y., Hammond, W. C., Ding, H., Mallick, R., Jiang, W., Xu, X., Shen, W. (2021). GPS Imaging of Vertical Bedrock Displacements: Quantification of Two-Dimensional Vertical Crustal Deformation in China. Journal of Geophysical Research: Solid Earth, 126(4).

Pan, Y., Jiang, W., Ding, H., Shum, C. K., Jiao, J., and Li, J. (2023). Intradecadal fluctuations and three-dimensional crustal kinematic deformation of the Tianshan and Pamir derived from multi-geodetic imaging. Journal of Geophysical Research: Solid Earth, 128, e2022JB025325.

Peltier, W. R., D. F. Argus, and R. Drummond. (2018). Comment on the paper by Purcell et al. 2016 entitled An assessment of ICE-6G_C (VM5a) glacial isostatic adjustment model, Journal of Geophysical Research: Solid Earth, 122.

Rinzin, S., Zhang, G., Sattar, A., Wangchuk, S., Allen, S. K., Dunning, S., and Peng, M. (2023). GLOF hazard, exposure, vulnerability, and risk assessment of potentially dangerous glacial lakes in the Bhutan Himalaya. Journal of Hydrology, 619, 129311.

Rao, W., and Sun, W. (2022). Uplift of the Tibetan Plateau: How to accurately compute the hydrological load effect? Journal of Geophysical Research: Solid Earth, 127, e2021JB022475.

Schneider, U., Becker, A., Finger, P., Rustemeier E., Ziese, M. (2022). GPCC Monitoring Product: Near Real-Time Monthly Land-Surface Precipitation from Rain-Gauges based on SYNOP and CLIMAT data.

Scanlon, B. R., Zhang, Z., Rateb, A., Sun, A., Wiese, D., Save, H., ... and Reedy, R. C. (2019). Tracking seasonal fluctuations in land water storage using global models and GRACE satellites. Geophysical Research Letters, 46(10), 5254-5264.

Swenson, S., Chambers, D., and Wahr, J. (2008). Estimating geocenter variations from a combination of GRACE and ocean model output. Journal of Geophysical Research, 113, B08410.

Tapley, B. D., Watkins, M. M., Flechtner, F., Reigber, C., Bettadpur, S., Rodell, M., ... and Velicogna, I. (2019). Contributions of GRACE to understanding climate change. Nature Climate Change, 9(5), 358-369.

Tangdamrongsub, N., Han, S. C., Jasinski, M. F., and Šprlák, M. (2019). Quantifying water storage change and land subsidence induced by reservoir impoundment using GRACE, Landsat, and GPS data. Remote Sensing of Environment, 233, 111385.

Taube, C. M. (2000). Three methods for computing the volume of a lake. Manual of Fisheries Survey Methods II: With Periodic Updates; Schneider, JC, Ed, 175-179.

Wang, X., Ding, Y., Liu, S., Jiang, L., Wu, K., Jiang, Z., and Guo, W. (2013). Changes of glacial lakes and implications in Tianshan, central Asia, based on remote sensing data from 1990 to 2010. Environmental Research Letters, 8(4), 044052.

Wang, H., Huang, Z., Wen, Z., and Luo, Z. (2022a). Lake Water Storage Changes in Northeast Hoh Xil Observed by Cryosat-2 and Landsat-5/7/8: Impact of the Outburst of Zhuonai Lake in 2011. IEEE Geoscience and Remote Sensing Letters, 19, 1-5.

Wang, Q., Yi, S., and Sun, W. (2017a). Precipitation-driven glacier changes in the Pamir and Hindu Kush mountains. Geophysical Research Letters, 44(6), 2817-2824.

Wang, Q., Yi, S., Chang, L., and Sun, W. (2017b). Large-scale seasonal changes in glacier thickness

942 across High Mountain Asia. Geophysical Research Letters, 44(20), 10-427.
943 Wang, Q., and Sun, W. (2022b). Seasonal cycles of High Mountain Asia glacier surface elevation
944 detected by ICESat-2. Journal of Geophysical Research: Atmospheres, 127, e2022JD037501.
945 Wahr, J., Molenaar, M., and Bryan, F. (1998). Time variability of the Earth's gravity field: Hydrological
946 and oceanic effects and their possible detection using GRACE. Journal of Geophysical
947 Research, 103(B12), 30205–30229.
948 Wen, Z, Rao W, Sun W. (2023). Contribution of loading deformation to the GNSS vertical velocity
949 field in the Chinese mainland, Geophysical Journal International, 233(3),1655–1670.
950 White, A. M., Gardner, W. P., Borsa, A. A., Argus, D. F., and Martens, H. R. (2022). A review of
951 GNSS/GPS in hydrogeodesy: Hydrologic loading applications and their implications for water
952 resource research. Water Resources Research, 58(7), e2022WR032078.
953 Woolway, R. I. and Merchant, C. J. Worldwide alteration of lake mixing regimes in response to climate
954 change. Nature Geoscience, 12, 271–276 (2019).
955 Woolway, R. I., Kraemer, B. M., Lenters, J. D., Merchant, C. J., O'Reilly, C. M., and Sharma, S.
956 (2020). Global lake responses to climate change. Nature Reviews Earth & Environment, 1(8),
957 388-403.
958 Wu, D., Yan, H., and Yuan, S. (2018). L1 regularization for detecting offsets and trend change points in
959 GNSS time series. GPS Solutions, 22(3), 1–5.
960 Wu, Y., Zheng, Z., Nie, J., Chang, L., Su, G., Yin, H., ... and Bo, W. (2022). High-Precision Vertical
961 Movement and Three-Dimensional Deformation Pattern of the Tibetan Plateau. Journal of
962 Geophysical Research: Solid Earth, 127(4), e2021JB023202.
963 Xu, Y., Li, J., Wang, J., Chen, J., Liu, Y., Ni, S., ... and Ke, C. (2020). Assessing water storage changes

964 of Lake Poyang from multi-mission satellite data and hydrological models. Journal of
965 Hydrology, 590, 125229.
966 Xu, Y., Lin, J., Zhao, J., and Zhu, X. (2021). New method improves extraction accuracy of lake water
967 bodies in Central Asia. Journal of Hydrology, 603, 127180.
968 Xu, F., Zhang, G., Yi, S., and Chen, W. (2022a). Seasonal trends and cycles of lake-level variations
969 over the Tibetan Plateau using multi-sensor altimetry data. Journal of Hydrology, 604, 127251.
970 Xu, N., Ma, Y., Wei, Z., Huang, C., Li, G., Zheng, H., and Wang, X. H. (2022b). Satellite observed
971 recent rising water levels of global lakes and reservoirs. Environmental Research Letters,
972 17(7), 074013.
973 Yao, F., Wang, J., Wang, C., and Crétaux, J. F. (2019). Constructing long-term high-frequency time
974 series of global lake and reservoir areas using Landsat imagery. Remote Sensing of
975 Environment, 232, 111210.
976 Yao, F., Livneh, B., Rajagopalan, B., Wang, J., Crétaux, J. F., Wada, Y., and Berge-Nguyen, M. (2023).
977 Satellites reveal widespread decline in global lake water storage. Science, 380(6646), 743-
978 749.
979 Yi, S., and Sun, W. (2014). Evaluation of glacier changes in high-mountain Asia based on 10 year
980 GRACE RL05 models. Journal of Geophysical Research: Solid Earth, 119(3), 2504-2517.
981 Yi S, Wang Q, Chang L, Sun W. (2016). Changes in Mountain Glaciers, Lake Levels, and Snow
982 Coverage in the Tianshan Monitored by GRACE, ICESat, Altimetry, and MODIS. Remote
983 Sensing. 8(10):798.
984 Yi, S., Song, C., Wang, Q., Wang, L., Heki, K., and Sun, W. (2017). The potential of GRACE
985 gravimetry to detect the heavy rainfall-induced impoundment of a small reservoir in the upper

Y ellow R iver. Water Resources Research, 53(8), 6562-6578.

Yi, S., and Sneeuw, N. (2021). Filling the data gaps within GRACE missions using Singular Spectrum Analysis. Journal of Geophysical Research: Solid Earth, 126, e2020JB021227.

Zhang, L., Yi, S., Wang, Q., Chang, L., Tang, H., and Sun, W. (2019). Evaluation of GRACE mascon solutions for small spatial scales and localized mass sources. Geophysical Journal International, 218(2), 1307-1321.

Zhang, G., Xie, H., Kang, S., Yi, D., and Ackley, S. F. (2011). Monitoring lake level changes on the Tibetan Plateau using ICESat altimetry data (2003–2009). Remote Sensing of Environment, 115(7), 1733-1742.

Zhang, G., Yao, T., Shum, C. K., Yi, S., Yang, K., Xie, H., ... and Yu, J. (2017). Lake volume and groundwater storage variations in Tibetan Plateau's endorheic basin. Geophysical Research Letters, 44(11), 5550-5560

Zhang, G., Chen, W., and Xie, H. (2019). Tibetan Plateau's lake level and volume changes from NASA's ICESat/ICESat-2 and Landsat Missions. Geophysical Research Letters, 46(22), 13107-13118.

Zhao, G., Li, Y., Zhou, L., and Gao, H. (2022). Evaporative water loss of 1.42 million global lakes. Nature Communications, 13(1), 3686.

Zhang, Y, Wang N, Yang X, Mao Z. (2022a). The Dynamic Changes of Lake Issyk-Kul from 1958 to 2020 Based on Multi-Source Satellite Data. Remote Sensing, 14, 157.

Zhang, Y., An, C. B., Zheng, L. Y., Liu, L. Y., Zhang, W. S., Lu, C., and Zhang, Y. Z. (2023). Assessment of lake area in response to climate change at varying elevations: A case study of Mt. Tianshan, Central Asia. Science of The Total Environment, 161665.

1008 Zhang S, Meng L, Zhao Y, Yang X and Huang A. (2022b). The Influence of the Tibetan Plateau
1009 Monsoon on Summer Precipitation in Central Asia. Frontiers in Earth Science, 10:771104.
1010 Zhong, Y., Wang, B., Zou, C. B., Hu, B. X., Liu, Y., and Hao, Y. (2017). On the teleconnection patterns
1011 to precipitation in the eastern Tianshan Mountains, China. Climate Dynamics, 49, 3123-3139.